Thermal Deformation Analysis of Tabbed Solar Cells Using Solder Alloy and Conductive Film

Md. Kamrul HASAN[1, 2], and Katsuhiko SASAKI[*3]

[1] Division of Human Mechanical Systems and Design, Graduate School of Engineering, Hokkaido University, Kita13, Nishi 8, Kita-ku, Sapporo, Hokkaido 060-8628

[2] Department of Mechanical Engineering, Chittagong University of Engineering and Technology, Chittagong - 4349, Bangladesh

[3] Department of Mechanical Engineering, Faculty of Engineering, Hokkaido University, Kita13, Nishi 8, Kita-ku, Sapporo, Hokkaido 060-8628

*Corresponding Author:
Katsuhiko SASAKI, PhD, Professor
Department of Mechanical Engineering, Faculty of Engineering, Hokkaido University
Kita13, Nishi 8, Kita-ku, Sapporo, Hokkaido 060-8628, Japan
Tel/Fax: +81-011-706-8376, E-mail:katsu@eng.hokudai.ac.jp

Keywords: solar cell, silicon wafer, cyclic thermal stress, FEA, solder alloy, conductive film

***Word count*:** 4233 words (Introduction through Conclusion)

***Manuscript Type*:** Original Research

Abstract

Finite element analysis (FEA) has been carried out with the aim of understanding the thermal deformation characteristics of two solar cell configurations. One of the solar cell models is tabbed by lead-free solder, the other model by conductive film (CF). A high temperature soldering process could weaken the bond and reduce the reliability of the cells because of the residual stress caused by the different thermal expansion coefficients of the materials. Moreover, solar irradiation generates temperature distribution across the surface of the solar cell, and the development of solar cells made of thinner crystalline silicon wafers will lead to the reduction in manufacturing costs. In this study, finite element analysis (FEA) of the manufacturing process has been carried out using both solder and CF bonding. Three temperature cycles were applied to analyze different environmental operating conditions and understand how thermal cycles affect the residual stress during actual service conditions. This investigation provides a comparison of thermal deformations between solder and CF bonded solar cells in order to understand which offers substantial reliability in the long term. Also this study explores the effects of various thicknesses of the silicon wafer on the residual stress and deformation of the solar cells.

1. Introduction

In recent years, photovoltaic power generation has been extending all over the world due to the scarcity of fossil fuels. Consumptions of fossil fuels lead to serious environmental issues such as air pollution since fossil fuels release carbon dioxide, nitrogen dioxide, sulphur dioxide, carbon monoxide etc. However, power from solar panel is one solution without the consequences of polluting the environment. A solar panel consists of a photovoltaic cell which converts solar power to electrical power directly. One of the issues of solar panels is that it undergoes cracking and fractures due to thermal deformation of the silicon wafer during solar to electrical power conversion. Solar panels are required to be used more than 30 years by considering the energy payback ratio (EPR). Therefore, the improvement in design considering the thermal deformation of solar cells is required.

Manufacturing companies try to lose some microns in silicon wafer thickness as a way to reduce costs and make solar cells more accessible. However, the trend toward thinner solar cells leads to problems of increased yield loss from breakage. Therefore, it is necessary to ensure the mechanical strength considering the effect of different geometric parameters on the thermal deformation within the solar cells.

Generally, a copper wire is used to interconnect solar cells in a solar panel via soldering. The solar cells and the wires are heated up to a high temperature of 220°C during the soldering operation [(1)]. Differences in the thermal and mechanical properties of the silicon used in cells and metal ribbon cause the residual stress around the bonding area, and lead to cracks and cell breakage after bonding [(2-3)]. The thinner wafers have higher risk of suffering from bowing and higher residual stress. One recent alternative is the use of a solar cell conductive film (CF) which enables low temperature bonding at 180°C [(4-5)]. CF is an adhesive tape with dispersed conductive particles, developed for connecting solar cells with metal ribbons.

Silicon wafer breakage has become a major concern of all semiconductor fabrication lines since silicon wafer is considered a brittle material, and high stresses are induced during the manufacturing process. Chen et al. reported an approach for characterizing silicon wafer failure strength using a simple drop test to understand the stress distribution in wafer bulk before failure [(6)]. Based on the multimodal Weibull distribution, a new expression taking into account the surface, edge, and bulk flaws has been proposed by Rupnowski to describe the strength of silicon wafers [(7)]. Significant changes in fracture strength are found as a result of metallization morphology and crystallinity of silicon solar cells. Surface and edge defects such as micro-cracks, grain boundaries, and surface roughness are the most probable sources of

mechanical strength degradation; reduction of potential micro-cracks leads to an increase of mc-silicon wafer fracture strength [8].

The plastic deformation of silicon wafers due to the thermal stress at high temperatures in integrated circuit (IC) fabrication can be controlled by process and equipment design [9]. Wafers with fully rounded profiles give the largest breakage energy and lowest wafer breakage ratio compared to edged counterparts [10]. The thermo-mechanical balance between cell and interconnector is an important issue for high performance and reliability of the modules [11]. The main parameters that affect the residual thermal stress of the cell are the temperature of the hot-air for soldering, cell thickness, soldering rod thickness, and soldering rod width [12]. The results indicate that the residual stress is mainly concentrated at the junction between the soldering track and the two edges of the cell. The increasing residual stress may cause damage to the wafer region near the electrode [13-16]. Therefore, the interconnection at lower temperature is needed to reduce the thermal stress due to soldering.

The stresses on thinner wafers during the manufacturing cycle have been analyzed by considering mechanical loads such as sawing, manual handling, liquid jets, transport systems and pick and place equipment [17]. In addition, FEA modeling has been used to investigate grinding and lapping of wire sawn silicon wafers [18]. It was reported that the temperature variation during slicing exhibited undesirable warp, micro cracks and nanotopography on wafer surfaces, which were responsible for brittle fracture [19-20]. In contrast, the cells have to withstand the tensile stresses under outdoor operation in the finished modules. These tensile stresses are induced by temperature changes and mechanical loads from wind and snow [21].

Solar irradiation will generate a temperature distribution across a PV module surface during operation under the sun. It is noted that a PV module has to endure many thermal cycles under ideal and abrupt weather conditions during its life cycle. A typical thermal cycle involves warm up and cool down of the module which leads to more severe stress challenge for the structure. Hence, a comparative study of thermal deformations between solder and CF bonded solar cells is necessary by considering the manufacturing process and the operating conditions. A finite element model of a three point bending test was built in an earlier study to investigate and understand the effect of bending stress on the electrical reliability of anisotropic conductive film (ACF) [22]. In addition, the effect of the bonding force on the failure behavior of the ACF joints under temperature fluctuation environment was also investigated. The main failure mode of the thermally shocked ACF joints was a conduction gap of the joints with low

bonding forces and adhesive matrix delamination of the joints with high bonding forces [23].

The present study aims to clarify thermal deformation of solar cells with different thicknesses of silicon wafer by considering thermal condition during manufacturing process and the used conditions under the sun. Sn-3.5Ag solder and CF are used to simulate the bonding interface and to carry out a comparison of the thermal deformation characteristics using FEM software.

The main objectives of this study are listed below:

1. Simulation of manufacturing process and using conditions of solar cells through FEM analysis, in order to determine the long term effects of residual stresses.
2. Compare the bonding materials, CF and solder, in order to determine which offers comparable reliability in the long term.
3. How different thicknesses of silicon wafers behave for both materials, in order to determine an adequate thickness.

2. Analysis Method

2.1 Basic FEM model

Finite element analysis was carried out by using ANSYS 14.5 (Ansys, Cecil Township, US). Due to the symmetry of the package geometries, only 1/4 of the solar cell assembly was modeled. The model built for the simulation consisted in three simple blocks. Each block represents a different material: silicon, copper and the bonding material in between. The symmetry conditions are applied in the z-axis in order to simplify the model. The model was adopted with 3-dimensional 8-node SOLID185 element which has plasticity, stress stiffening, large deflection, and large strain capabilities. Finer mesh is applied in the central part of the solar cell as the maximum stress point occurred in the tabbing section of the cell**.** The dimension of silicon solar cell was considered for this analysis to be 152mm × 152mm × 0.2mm. The schematics of the FEM model are exhibited in Fig. 1. Two FEM models were developed for the different bonding materials solder and CF. All the dimensions are shown in Table 1.

2.1.1 Assumptions and restrictions

In order to work with a simple model, some assumptions had to be made. All materials are bonded from the beginning. Any thermal expansion affects the surrounding materials from time zero. In a real process, materials expand independently during the first part of the manufacturing process and become bonded during the cooling

process (when solder solidifies or when conductive film reaches its adhesion point). However, this would have required an adjustment to the contact surfaces at a certain point during the analysis. Although it is possible, the complexity of the model increases dramatically. Solder was ignored in the conductive film model. In a real CF cell, a very thin solder layer exists in the tabbing area. Also, the rest of the structure of a typical solar module (frame, glass, etc.) was ignored. Using symmetry boundary conditions in two of the borders a simplified model of only one quarter of a solar cell was built. No constrains were imposed on the open borders of the silicon wafer.

2.2 The variable

To understand the effect of changes in the thickness of the silicon on the residual stress and deformation, four thicknesses of silicon wafer were considered in this study, as shown in Table 2. Each bonding material (solder or CF) was applied in four geometrical conditions for a total of 8 cases for analysis and comparison.

2.3 Material Properties

The properties of solder, CF, and silicon were chosen as follows.

The total strain of solder is expressed as Eq.1.

$$\mathcal{E} = \mathcal{E}_e + \mathcal{E}_p + \mathcal{E}_c \quad (1)$$

where $\mathcal{E}_e$ is the elastic strain, $\mathcal{E}_p$ is the plastic strain, and $\mathcal{E}_c$ is the creep strain.

The plastic strain was determined from the bilinear kinematic hardening rule. This rule assumes that the total stress amplitude is equal to twice the yield stress as shown in Fig. 2. This rule can be considered as a Bauschinger effect observed in the cyclic tensile and compressive loading.

The temperature dependent properties of solder were calculated from the stress-strain diagrams [24].

The Creep strain of solder can be expressed by Norton's law for steady-state creep considering temperature dependency,

$$\mathcal{E}_c = C\sigma^n \quad (2)$$

where σ is the equivalent stress, C and n are constants expressed as a function of temperature T as in Eq.3 and Eq.4, respectively.

$$C = 2.49 \times 10^{-9} exp(-3.99 \times 10^{-2} T) \quad (3)$$

$$n = 2.49 \times 10^{-2} T - 5.09 \times 10^{-1} \quad (4)$$

A Maxwell viscoelastic model was used for CF to predict the stress or strain interactions under different

loading conditions. The Maxwell model can be represented by a purely viscous damper and a purely elastic spring connected in series.

In this model, the relaxation modulus, *G(t)* is determined by the Eq.5.

$$G = G_e + \Sigma G_i exp(-t/t_i) \quad (5)$$

Material constants G_e, G_i, and t_i were identified by dynamic viscoelasticity test as shown in Table 3.

The Williams-Landel-Ferry Equation (or WLF Equation) is used as time-temperature superposition principle to determine the stress relaxation behavior of CF [25]. The WLF equation has the form as Eq.6,

$$log a_T = \frac{-C_1(T-T_R)}{C_2+(T-T_R)} \quad (6)$$

Where a_t is the shift factor and C_1, C_2 are constants.

For silicon, only elastic properties were considered as it is a brittle material. The Young's modulus and Poisson's ratio of silicon were 167GPa and 0.22, respectively [26].

2.4 Analysis Condition

First, FEM analysis was carried out for the manufacturing process using solder bonding and CF bonding. The Sn-3.5Ag bonding consisted of heating from 298K to 493K for 15 seconds, then cooled immediately to 298K in the next 15 seconds. In the case of CF bonding, heating was up to 453K and a pressure of 1MPa was applied during the whole process. Figure 3(a) exhibits the thermal profiles of the manufacturing process for solder bonding, while Fig. 3(b) shows the thermal profiles of the CF bonding.

As for the used condition, the effects of the thermal cycle and the thickness of silicon wafer are analyzed.

Three temperature cycles of 288~338 K, 278~318 K and 298~338 K as shown in Fig. 4 were applied to the analysis to understand the effect of different thermal cycles on the residual stress developed during manufacturing of the solar cell. The temperature increase and decrease rates are 50K/hour for the temperature cycles of 288~338 K and 40K/hour for 278~318 K and 298~338 K. Table 4 shows the temperature change for a simulation of 3 days. The thickness of silicon wafer considered in this case was 200μm. A thermal cycle 288~338 K was applied to the analysis to clarify the effect of changes in the thickness of silicon on stress and strain distributions within the solar cell.

3. Analysis Result

3.1 Basic Model

The effect of two different bonding materials on solar cells deformation is explored in this section.

First, the analysis was carried out for manufacturing process using solder bonding and CF bonding. Thereafter, three temperature cycles considering different environmental operating conditions were applied to the analysis to understand how different thermal cycles affect the residual stress. The data was taken at the same time of analysis, in the same node for all models.

3.1.1 Manufacturing process

Results of the equivalent stress and strain were taken at 30 seconds of the manufacturing process to compare the effect of different bonding materials on the solar cells before exposing it to sunlight for its operation, as the temperature distribution redistributes the residual stress. The measurements were made in ANSYS 14.5 as time steps.

The equivalent stress distribution of the silicon after manufacturing for both solder bonding and CF bonding is exhibited in Fig.5. The maximum equivalent stress of silicon developed for solder bonding is 95.2 MPa while it is 19.5 MPa for CF bonding. It can be observed that the maximum equivalent stress for solder bonding is about 5 times higher compared to CF bonding. Hence, the lower bonding temperature of CF in the manufacturing process makes it possible to have lower stress in the silicon. The residual stress was mainly concentrated at the edge of the tabbing track and the maximum residual stress observed at the margin of the cell edge.

In addition, the maximum equivalent strain of silicon is also 5 times higher for solder bonding than that of the CF bonding. Therefore, it can be said that CF bonding has a much greater reliability than solder bonding.

3.1.2 Usage process

The analysis of the cells during usage was carried out to understand the long-term effects of residual stresses that generated during the manufacturing process. Three temperature cycles of 278~318 K, 298~338 K and 288~338 K were applied to the analysis The times considered during the analysis were six months for solder and one month for the CF bonded cell.

Figure 6 shows the changes of stresses and strains of silicon with time for solder bonding. In this case the, stress in the silicon decreases with increase in temperature cycle. The decreasing order of the cycles for stress and strain are 288~338 K, 278~318 K and 298~338 K. In the case of the CF, the changes of stress and strain are negligible due to the fact that the strain is negligible in value and the decreasing order of the cycles are 278~318 K, 288~338 K and 298~338 K.

The variation of equivalent stress and strain of solder is shown in Fig. 7. In the case of CF, strain of

solder increases after passing 35 days for the cycle 278~318 K and about 60 days for the cycles 298~338 K and 288~338 K. The increasing trend of strain is sharper for the cycle of 278~318 K compared to the other two cycles. The cycle of 288~338 K has a higher strain in first 55 days. However it becomes lower with time compared to the cycle of 278~318 K. It is noted that the stress of solder is similar for the cycles of 278~318 K and 288~338 K but lower for the cycle of 298~338 K.

3.1.3 Long term usage conditions

In order to understand the creep deformation characteristics of solder in the long term, the analysis of the basic model was carried out for two years (730 days) under representative conditions. The thermal cycle used for the analysis was 288-338 K.

The variation of equivalent stress of solder with time is shown in Fig. 8(a). which indicates that the change of stress is not significant for the first year of usage, whereas stress decreases after a year. The strain increases sharply after 60 days during the first year as shown in Fig. 8(b). The increasing tendency towards more strain and plastic deformation with no change in stress is due to the creep of solder. The strain arises owing to CTE mismatches between joined materials in solar cell assemblies that expand and contract to different lengths as the temperature changes. It is noted that, the rate of change of strain becomes slower after a year. The equivalent strain of solder after two years of use is 6.68 [%]. However the creep strain has a tendency to saturate after about 400 days.

3.2 Changes in the thickness of silicon

This section explores the effect of varying the silicon wafer thickness on the residual stress and deformation considering the manufacturing and using process of solar cells.

3.2.1 Manufacturing process

A greater amount of stress is obtained for thinner cells in case of solder bonding. The effects of varying the silicon thicknesses on the maximum stress, and strain of silicon are shown in Fig. 9. The maximum equivalent stresses developed in solder bonded silicon of 50, 100, 150 and 200μm thickness are about 260, 167, 122 and 95MPa, respectively, while in CF bonded silicon they are about 66, 38, 25 and 20MPa, respectively. It should be noted that the maximum obtained stress for CF is much lower compared to the minimum obtained stress for solder. For the thinnest silicon of 50μm, the maximum strain is 0.16[%] for solder bonding, while it is 0.04[%] for CF bonding. In the case of 200μm silicon, the maximum strain for solder is 0.057 [%] and 0.012[%] for CF. Results show that, for all materials and thicknesses, CF bonding results in much lower stresses than solder. With decreasing silicon thickness, silicon undergoes an

increase in strain and stress, as expected. The reduced thickness of the wafer implies that it is more flexible, which means that the strain is higher for the same thermal load. However the rate of change of silicon stress with respect to silicon thickness is much lower when CF is used. It is because; lower thickness wafer is more susceptible to higher temperature of soldering than the CF bonding.

The effects of changes in the silicon thicknesses on maximum stress and strain in the bonded materials are shown in Fig. 10. For the thinnest silicon of 50μm, the maximum stress and strain of solder are observed to be 22.7 MPa and 6.33[%], respectively, while 1.42 MPa and 7.65[%] for CF. In case of 200μm silicon, the maximum stress and strain for solder are observed to be 23.8 MPa and 7.42[%], while 1.41 MPa and 7.63[%] for CF.

It is clear that the maximum stress and strain for solder bonding are much higher than for CF bonding. Solder bonding may not be a suitable option when considering the current trend of reducing silicon thickness. A manufacturing process based on CF bonding has much more reliability compared to solder bonding for all thicknesses of silicon.

3.2.2 Usage process

The variation of equivalent stress and strain of silicon bonded by solder is shown in Fig. 11. The equivalent stress on the solar cell is reduced for all thicknesses of silicon passing through the temperature cycles. The decreasing order of the stress and strain for thicknesses of silicon is 50, 100, 150 and 200μm. The rates of variation of stress and strain are much higher for thin silicon wafers. While, in the case of CF, there is quite a small stress increase, then afterwards, there is no significant change of stress and strain with time as shown in Fig. 12.

The variation of equivalent stress and strain of solder is shown in Fig. 13. For the bonding materials, there is no significant change of CF stress and strain with time. However for solder, strain increases with a decrease in silicon thickness after some days, which is due to the creep properties of the solder. The change of strain with time is much rapid for thinner silicon and the strain increases sharply for 50 μm thickness of silicon. The stress of solder has no significant change with thickness of silicon. The residual stress and strain values of the CF are lower for the thinner silicon wafers. It is noted that creep deformation accumulates in the solder rather than in the more brittle components to which it is attached.

3.3 Discussions

This study was aimed to simulate the manufacturing process and usage conditions of two solar cell configurations using FEM software. In addition, different silicon wafer thicknesses were considered in

order to analyze the long-term development of induced stresses. The first solar cell model was considered to be tabbed by a lead-free solder. The solder joint was sandwiched in between the copper wire and the silicon wafer. The large life span of solar cells and its continuous loading and unloading led to creep deformation which was an important phenomenon to be considered. It is noted that high stresses were induced in the manufacturing process due to the higher bonding temperature of solder. Identical strain and stress contours were obtained for silicon since this material is modeled as perfectly elastic. In addition, the analysis identified the critical locations on the cell which were potentially susceptible to structural failure after a few thousand thermal cycles due to the creep strain. Hence, the real challenge came from the analysis to determine the effects of creep and stress relaxation in the long term as two years (730 days) of usage conditions were applied. It is noted that the equivalent strain of solder at two years of usage was 6.683[%]. In addition, the change in residual stress in wafer exhibited inverse relationship with the thickness of the wafer. Hence, solder bonding was not considered be a suitable option for current trend of reducing silicon thickness since the reliability was decreased with thin wafers due to the higher temperature manufacturing process.

The second solar cell model was bonded by CF taking viscoelastic properties into account. It is noted that the maximum equivalent stresses of CF bonded cell were fairly below the stresses of the solder bonded cell due to the lower temperature bonding. In addition, CF provided low stress level compared to all thicknesses of silicon regarding the usage conditions. Therefore, CF bonding was considered to be a potential option to tab solar cells such as thin and next generation solar cells (100μm – 50μm).

There were a few limitations to the analysis; the constitutive model and the estimation of the fatigue failure was not considered in this paper.

The accuracy of the structural analysis usually depends on the constitutive model employed in the analysis. Herein, the bi-linear stress-strain relation for plastic strain and Norton's law for creep strain were used for the solder alloy since these constitutive models do not need a long computational time to obtain the results. However, as one of the authors has previously pointed out [27], a precise constitutive model explaining both the nonlinearity of the stress-strain relation and the creep curve are required to obtain the more physically based results, though the longer computational time is required. The construction of a new constitutive model to obtain the more accurate data will be conducted in the future.

The estimation of the fatigue failure of solders has also already been discussed by one of the authors [28]. A prediction method was proposed using the creep strain amplitude after a few cycle of the cyclic

loading obtained from the analysis. It was reported that the creep strain amplitude has an advantage to estimate the fatigue failure of the solder alloy. This method may also be employed for the estimation of failure of the solar cells in future work.

The fatigue failure of solar cells under an actual usage conditions should also be addressed to confirm the accuracy of the results of the paper. However, it is necessary to investigate the fatigue failure over a period of twenty to thirty years. Therefore, an experimental method based on an accelerated test such as HALT (highly accelerated limit test) should be employed [29].

Regarding the CF bonding, there is not enough research work for an estimation of the fatigue failure. Therefore, to confirm the accuracy of the results obtained in this paper, basic experiments related to fatigue failure should be conducted for CF bonding.

4. Conclusion

The present study performed a finite element analysis of manufacturing process and using conditions of solar cells to investigate the effect of various thicknesses of silicon wafer and temperature cycles on the deformation and residual stress. Sn-3.5Ag solder and CF were employed as the bonding interface of the solar cells. The results are summarized as follows:

(1) As for the manufacturing process, considering all thicknesses of silicon cells, both the residual stress and strain are much lower for CF compared to the solder bonded solar cell. Hence, CF bonding seems to be a promising method to tab solar cells. The residual stress was mainly concentrated at the edge of the tabbing track of the cells and the maximum residual stress observed at the margin of the cell edge.

(2) As for the usage conditions considered, there is no significant change in either stress and strain with time for CF bonding, while, in the case of solder bonding, the stress on the solar panel decreases due to the imposed temperature cycles, however, the change in stress becomes small with time. The strain of the solder increases after some days due to creep deformation. However, the lower stresses and strains in CF bonded joints do not ensure the reliability over 30 years, as other factors may also play a role.

(3) The trend toward thinning cells may lead to an increase in the breakage risk of solar cells due to excessive residual stress during soldering. Even though silicon stresses increase as wafers become thinner, CF bonding still offers lower stresses and it is clearly the comparable manufacturing process

335 when using thin solar silicon wafers.

336

337 **Acknowledgements**

338 The data of viscoelastic deformation of CF was given by Mr. Yasuhiro SUGA from Dexerials
339 Corporation. The authors gratefully acknowledge his support.

340

Reference

(1) A.M. Gabor, M. Ralli and S. Montminy. Soldering induced damage to thin si solar cells and detection of cracked cells in modules, 21st European photovoltaic Solar Energy Conference, Dresden, 2006.

(2) X.F. Brun and S.N. Melkote. Analysis of stresses and breakage of crystalline silicon wafers during handling and transport. Journal of Solar Energy Materials & Solar Cells, 93, 1238-1247, 2009.

(3) J. Wendt, M. Trager, M. Mette, A. Pfennig, and B. Jaeckel, The link between mechanical stress induced by soldering and micro damages in silicon solar cells, 24th European Photovoltaic Solar Energy Conference, Germany, ISBN: 3-936338-25-63420–3423, 2009.

(4) J.W. Kim, J.M. Koo and C.Y. Lee. Thermal degradation of anisotropic conductive film joints under temperature fluctuation. Journal of Adhesion & Adhesives, 28, 314-320, 2008.

(5) P.A. Wang, Industrial challenges for thin wafer manufacturing, Proc. 4th World Conference on Photovoltaic Energy Conversion, Waikoloa, HI, USA, 1, IEEE, Piscataway, 1179-1182, May 2006.

(6) P. Chen, M. Tsai and W. Yeh. Relationship between wafer fracture reduction and controlling during the edge manufacturing process. Journal of Microelectronic Engineering, 87, 1809–1815, 2010.

(7) P. Rupnowski and B. Sopori. Strength of silicon wafers: fracture mechanics approach. International Journal of Fracture, 155, 67-74, 2009.

(8) V.A. Popovich, A.Yunus and M.Janssen, Effect of silicon solar cell processing parameters and crystallinity on mechanical strength. Solar Energy Materials & Solar Cell, 95, 97-100, 2011.

(9) A. Fischera, Th. Grabollaa and H. Richtera. Mechanical strength of 300 mm diameter silicon wafers at high temperatures: modeling and simulation. Journal of Microelectronic Engineering, 45, 209–223, 1999.

(10) P. Chen, M. Tsai and W.Yeh. Relationship between wafer edge design and its ultimate mechanical strength,. Journal of Microelectronic Engineering, 87, 2065–2070, 2010.

(11) Y. Zemen, T. Prewitz, T. Geipel, S. Pingel, J. Berghold. The impact of yield strength of the interconnector on the internal stress of the solar cell within a module, 25th European Photovoltaic Solar Energy Conference and Exhibition / 5th World Conference on Photovoltaic Energy Conversion, Valencia, Spain, 4073-4078, 6-10 September 2010.

(12) C. Lai, C. Su and K. Lin. Analysis of the thermal stress and warpage induced by soldering in monocrystalline silicon cells. Journal of Applied Thermal Engineering 55, 7-16, 2013.

(13) C.H. Chen, F.M. Lin and H.T. Hu. Residual stress and bow analysis for silicon solar cell induced by soldering. International symposium on solar cell technologies, Taipei, December 2008.

(14) L. Yu, Y. L. Jiang and S. K. Lu. 3D FEM for sintering of solar cell with boron back surface field based on solidwork simulation. IERI Procedia 1 Singapore, 81 – 86, 2012.

(15) P. Chen, M. Tsai and W. Yeh. Relationship between wafer fracture reduction and controlling during the edge manufacturing process. Journal of Microelectronic Engineering, 87, 1809–1815, 2010.

(16) L. Bittoni. Aluminum pastes suitable for wide range thin crystalline silicon solar cells processing blistering and bowing effects reduction. 21st EPSEC, Dresden, 818-821, 2006.

(17) P.A. Wang. Industrial challenges for thin wafer manufacturing, Proc. 4th World Conference on Photovoltaic Energy Conversion, Waikoloa, HI, USA, 1, IEEE, Piscataway, 1179-1182, 2006.

(18) WW.J. Liu, Z.J. Pei and X.J. Xin. Finite element analysis for grinding and lapping of wire-sawn silicon wafers. Journal of Materials processing technology, 129, 2-9, 2002.

(19) S. Bhagavata and I. Kao. A finite element analysis of temperature variation in silicon wafers during wiresaw slicing. International Journal of Machine Tools & Manufacture, 48, 95–106, 2008.

(20) C. Funke, S. Wolf and D. Stoyan, Modeling the tensile strength and crack length of wire-sawn silicon wafers. Journal of Solar Energy Engineering, 131, 011012-1, 2009

(21) P. Grunow, P. Clemens and V. Hoffmann. Influence of micro cracks in multi-crystalline silicon solar cells on the reliability of PV modules. 20th European Photovoltaic Solar Energy Conference, Barcelona, Spain, 2380-2383, June 2005.

(22) M.J. Rizvi, Y.C. Chan and C. Bailey. Study of anisotropic conductive adhesive joint behavior under 3-point bending. Journal of Microelectronics Reliability, 45, 589–596, 2005.

(23) J.W. Kim, J.M. Koo and C.Y. Lee. Thermal degradation of anisotropic conductive film joints under temperature fluctuation. Journal of Adhesion & Adhesives, 28, 314-320, 2008.

(24) Factual Database on Tensile and Low Cycle Fatigue Properties of Sn-37Pb and Sn-3.5Ag Solders, The Society of Materials Science, Japan, ISBN 4-901381-13-X, 2001.

(25) M. L. Williams, R. F. Landel, J. D. Ferry. The temperature dependence of relaxation mechanisms in amorphous polymers and other glass-forming liquids. Journal of the American Chemical Society, 77 (14), 3701–3707, 1955.

(26) W. N. Sharpe, Jr. B. Yuan, and R. Vaidyanathan. Measurements of young's modulus, poisson's ratio, and tensile strength of polysilicon, Proceedings of the Tenth IEEE International Workshop on Micro Electro Mechanical Systems, Nagoya, Japan, 424-429, 1997.

(27) K. Ohguchi, K. Sasaki, and M. Ishibashi, A quantitative evaluation of time-independent and time-dependent deformations of lead-free and lead-containing solder alloys, Journal of Electronic Materials, 35(1), 132-139, 2006.

(28) K. Ohguchi, and K. Sasaki, Investigation of effect of creep strain on low-cycle fatigue of lead-free solder by cyclic loading using stepped ramp waves, Journal of Electronic Packaging, 132, 041010-1-7, 2010.

(29) Y.-S. Chen, and L. H. Chuong, Efficiency improvement of the highly accelerated life testing system by using multiple hammers, Journal of Mechanical Science and Technology, 28 (12), 4815-4831, 2014.

Figures Legends

Fig. 1: One quarter FEM model of the solar cell.

Fig. 2: Schematic diagram of bilinear kinematic hardening law.

Fig. 3: Temperature conditions of manufacturing process. (a) Solder bonding (b) CF bonding

Fig. 4: Temperature change during using conditions. (a)288K↔338K (b)278K↔318K (c)298K↔338K

Fig. 5: Equivalent stress of silicon. (a) Solder bonding (b) CF bonding

Fig. 6: Equivalent stress and strain of solder bonded silicon during using process. (a) Equivalent stress (b) Equivalent strain

Fig. 7: Equivalent stress and strain of solder during using process. (a) Equivalent stress (b) Equivalent strain

Fig. 8: Equivalent stress and strain of solder during two years of using process. (a) Equivalent stress (b) Equivalent strain

Fig. 9: Effect of silicon thickness on the stress and strain of silicon. (a) Equivalent stress of silicon. (b)

Equivalent strain of silicon.

Fig. 10: Effect of silicon thickness on the stress and strain of bonding materials. (a) Equivalent stress of silicon. (b) Equivalent strain of silicon.

Fig. 11: Effect of silicon thickness on solder bonded silicon during using process. (a) Equivalent stress of silicon. (b) Equivalent strain of silicon.

Fig. 12: Effect of silicon thickness on CF bonded silicon during using process. (a) Equivalent stress of silicon. (b) Equivalent strain of silicon.

Fig. 13: Effect of silicon thickness on solder during using process. (a) Equivalent stress of silicon. (b) Equivalent strain of silicon.

Fig. 1 (a)

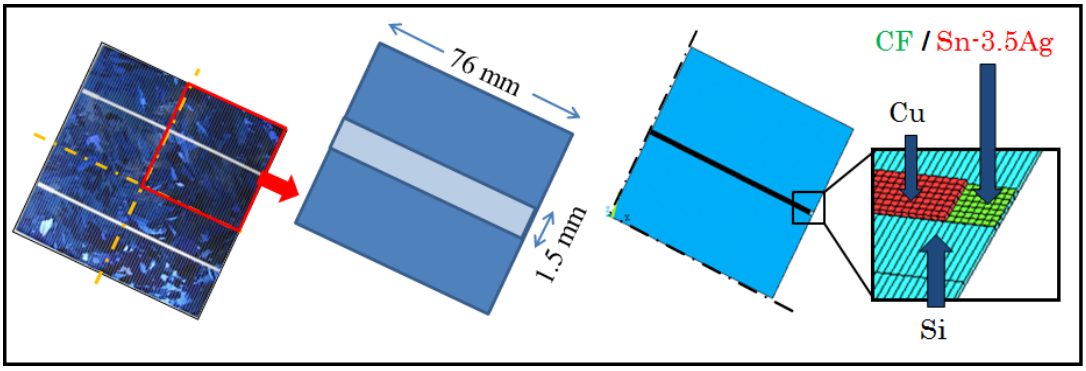

Fig. 2

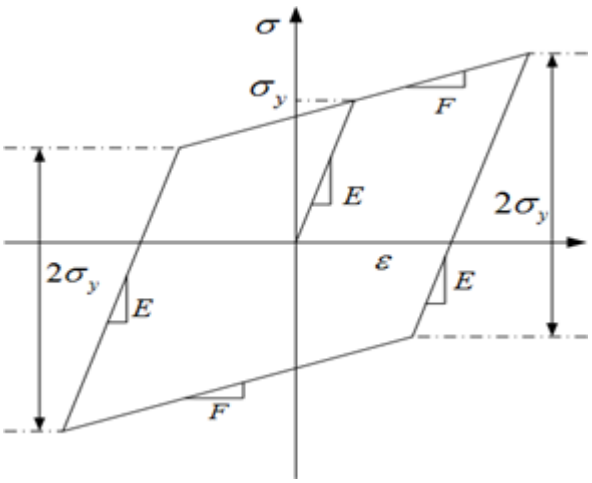

Fig. 3 (a)

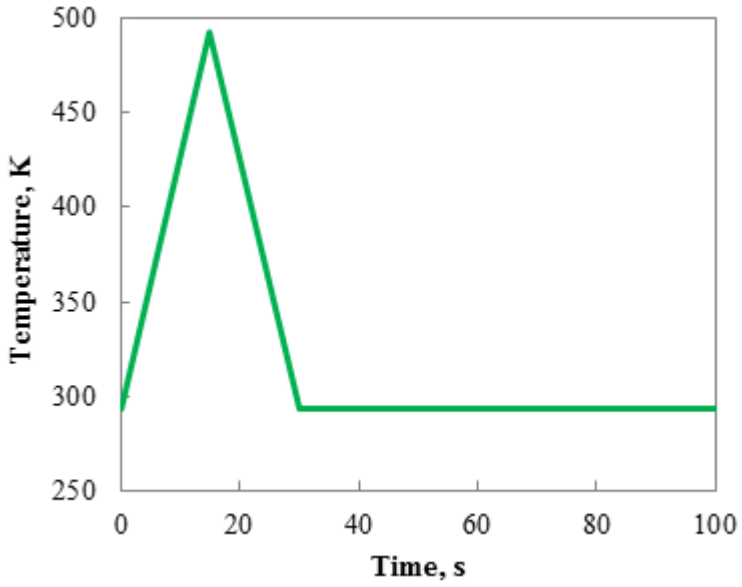
500
450
400
350
300
250
Temperature, K
0
20
40
60
80
100
Time, s

Fig. 3 (b)

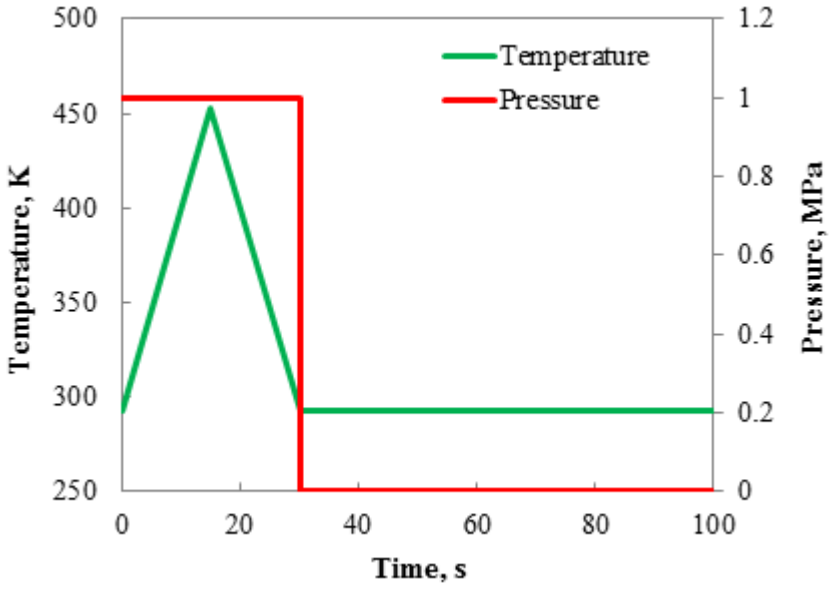
500
450
400
350
300
250
Temperature, K
1.2
1
0.8
0.6
0.4
0.2
0
Pressure, MPa
Temperature
Pressure
0
20
40
60
80
100
Time, s

Fig. 4

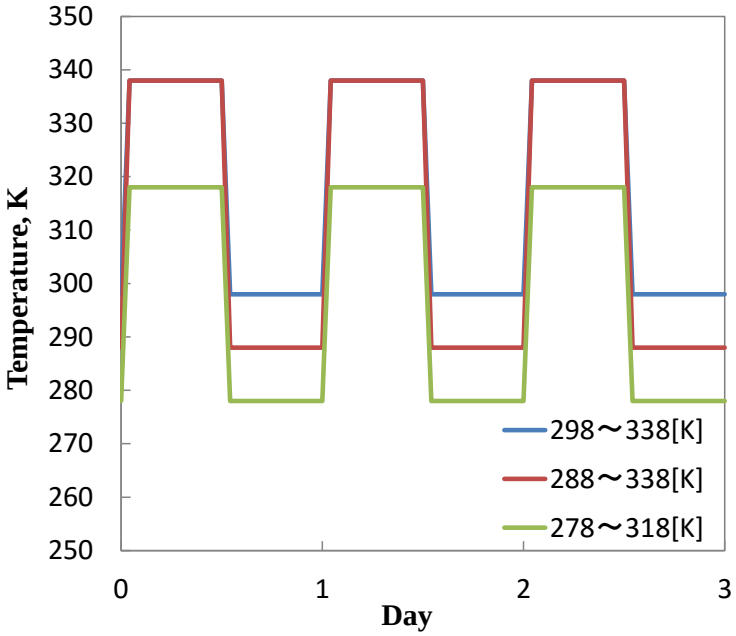
350
340
330
320
310
300
290
280
270
260
250
Temperature, K
0
1
2
3
Day
298～338[K]
288～338[K]
278～318[K]

Fig. 5 (a)

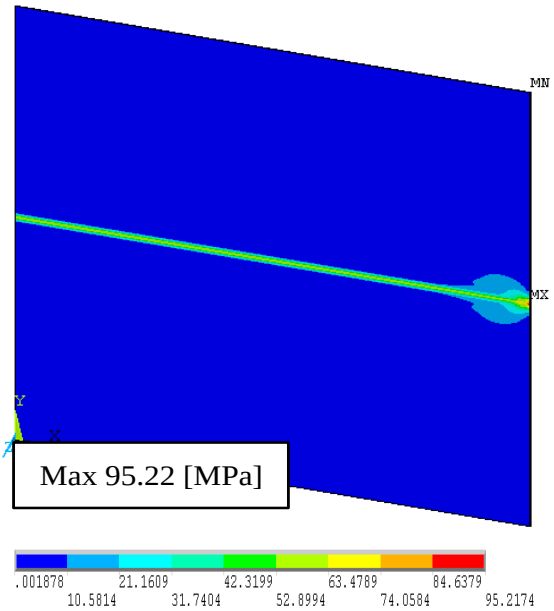
MN
MX
Y
Z
X
Max 95.22 [MPa]
.001878
10.5814
21.1609
31.7404
42.3199
52.8994
63.4789
74.0584
84.6379
95.2174

Fig. 5 (b)

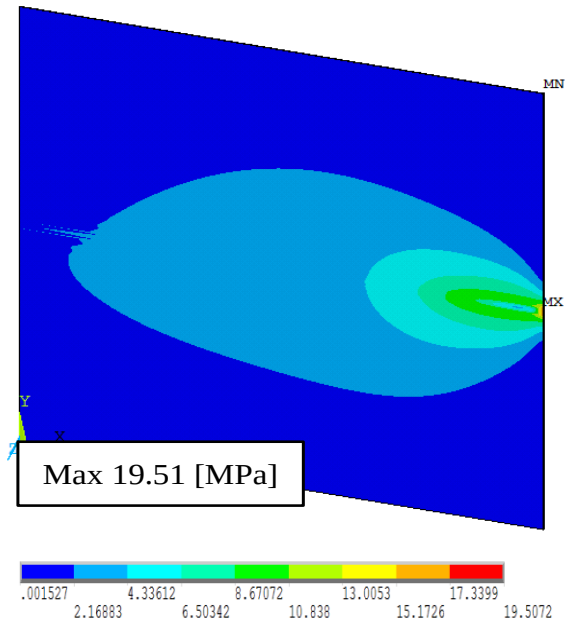
MN
MX
Y
Z
X
Max 19.51 [MPa]
.001527
2.16883
4.33612
6.50342
8.67072
10.838
13.0053
15.1726
17.3399
19.5072

Fig. 6 (a)

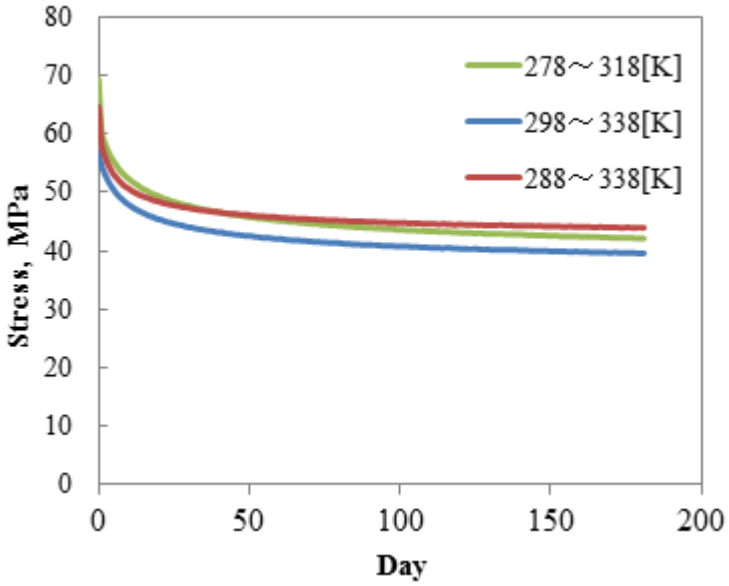
80
70
60
50
40
30
20
10
0
Stress, MPa
0
50
100
150
200
Day
278～318[K]
298～338[K]
288～338[K]

Fig. 6 (b)

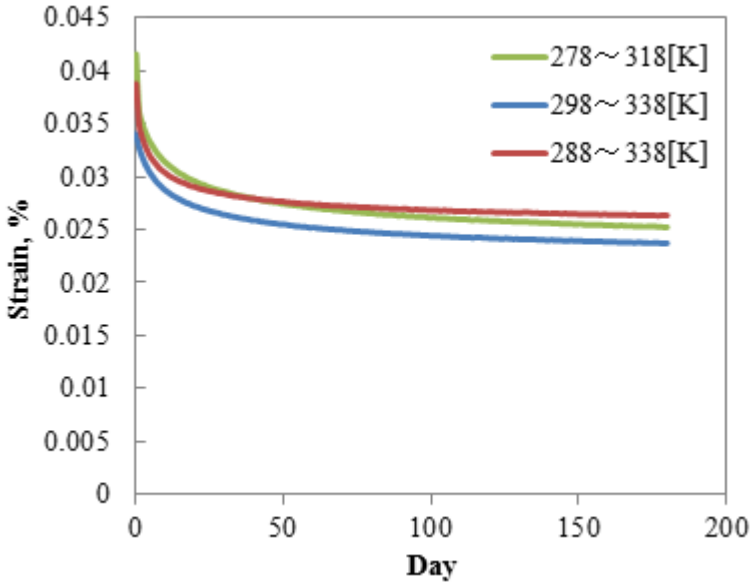
0.045
0.04
0.035
0.03
0.025
0.02
0.015
0.01
0.005
0
Strain, %
0
50
100
150
200
Day
278～318[K]
298～338[K]
288～338[K]

Fig. 7 (a)

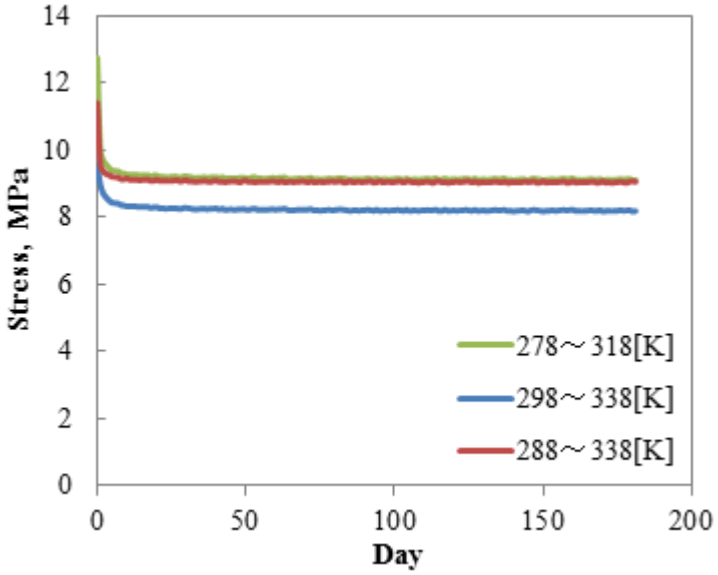
Stress, MPa
Day
278～318[K]
298～338[K]
288～338[K]

Fig. 7 (b)

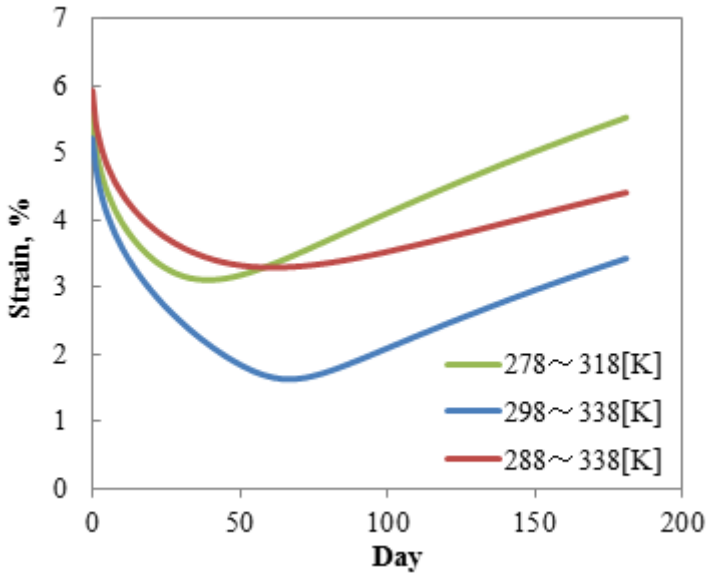
Strain, %
Day
278～318[K]
298～338[K]
288～338[K]

Fig. 8 (a)

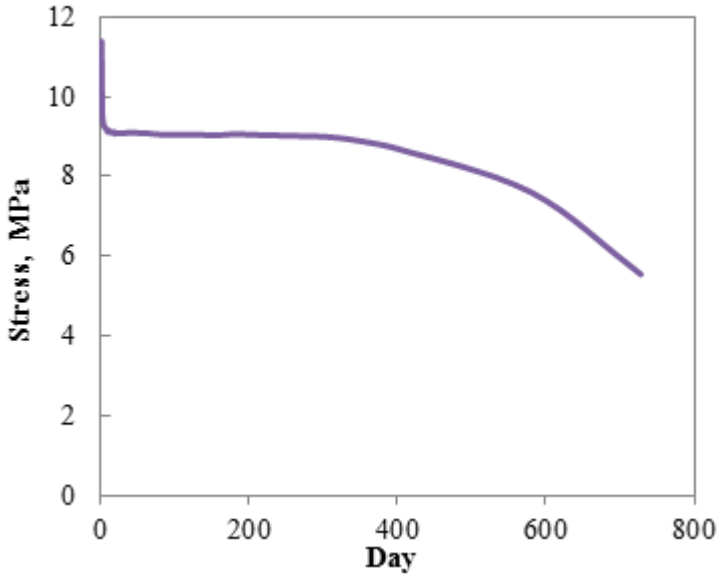
Stress, MPa
12
10
8
6
4
2
0
0
200
400
600
800
Day

Fig. 8 (b)

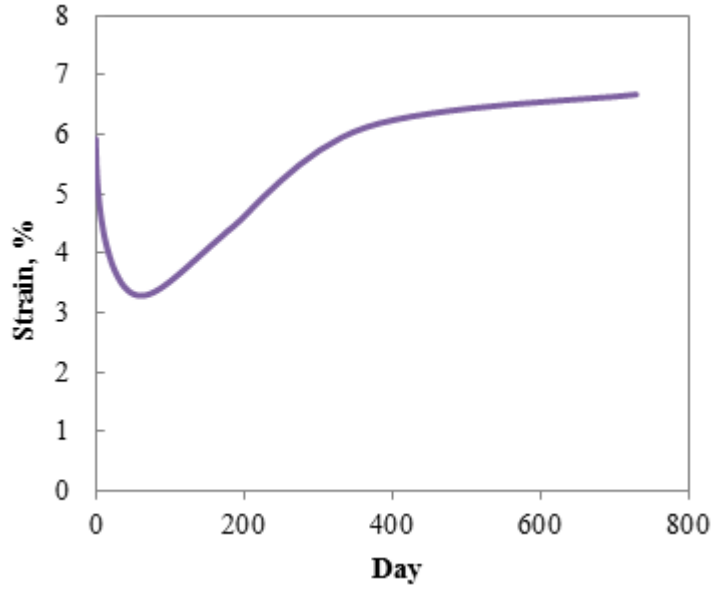
Strain, %
8
7
6
5
4
3
2
1
0
0
200
400
600
800
Day

Fig. 9 (a)

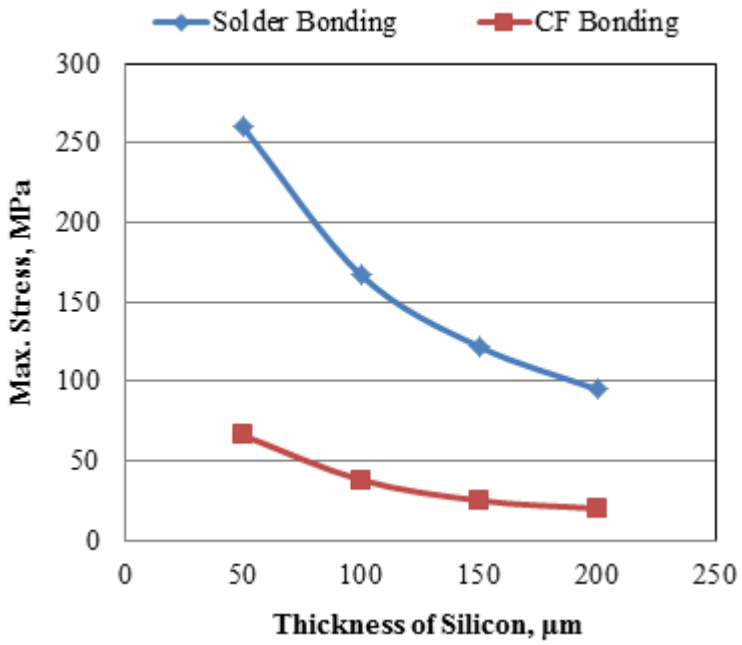
Solder Bonding
CF Bonding
Max. Stress, MPa
300
250
200
150
100
50
0
0
50
100
150
200
250
Thickness of Silicon, µm

Fig. 9 (b)

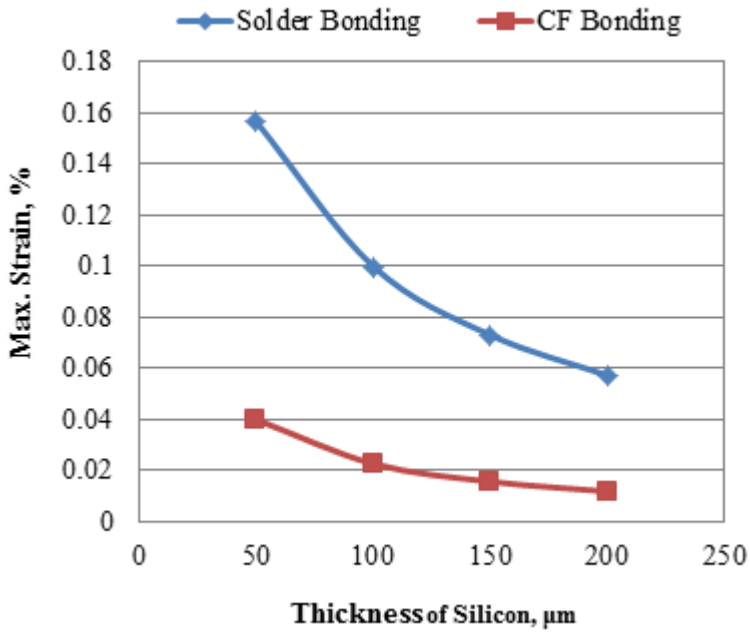
Solder Bonding
CF Bonding
Max. Strain, %
0.18
0.16
0.14
0.12
0.1
0.08
0.06
0.04
0.02
0
0
50
100
150
200
250
Thickness of Silicon, µm

Fig. 10 (a)

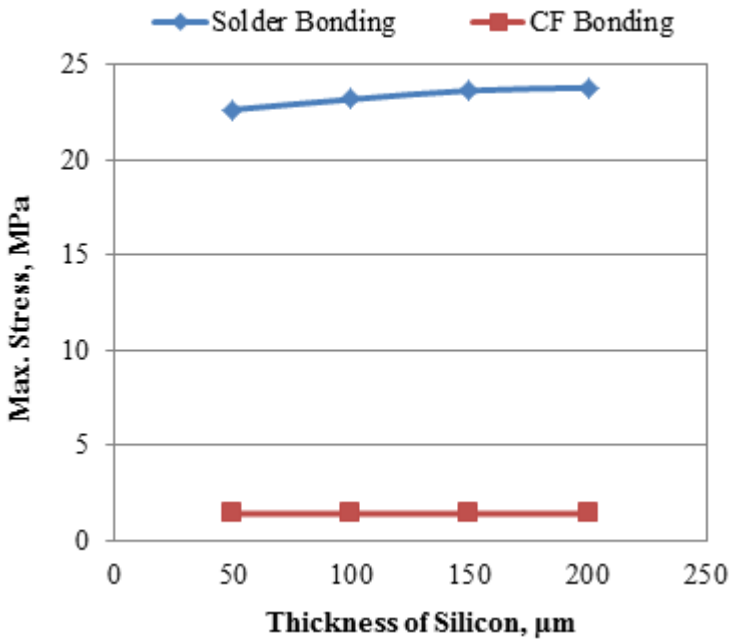

Fig. 10 (b)

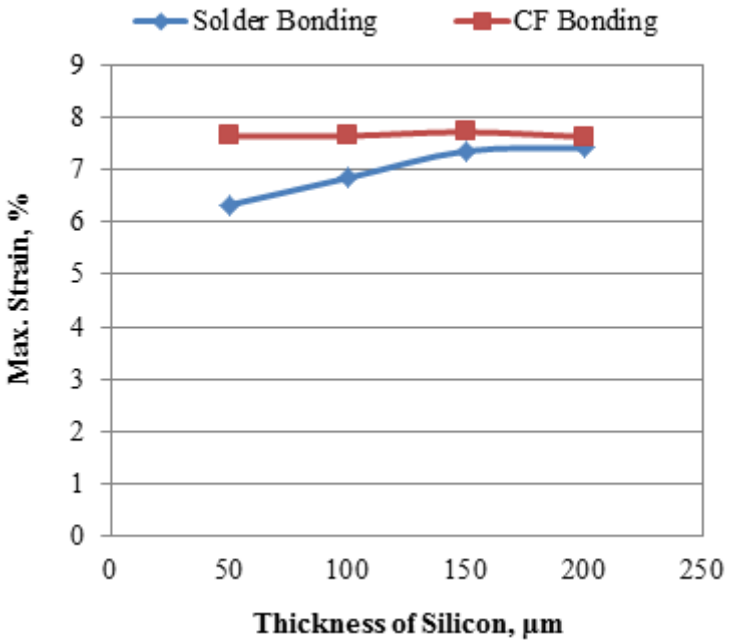

Fig. 11 (a)

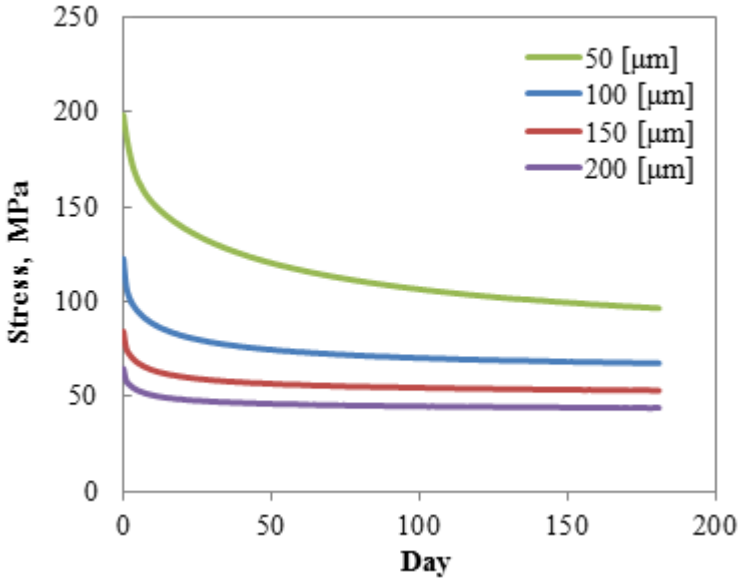

Fig. 11 (b)

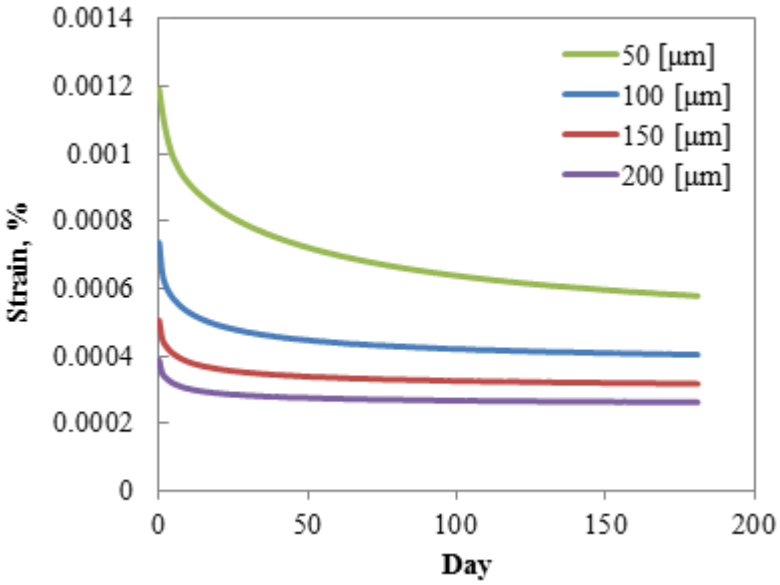

Fig. 12 (a)

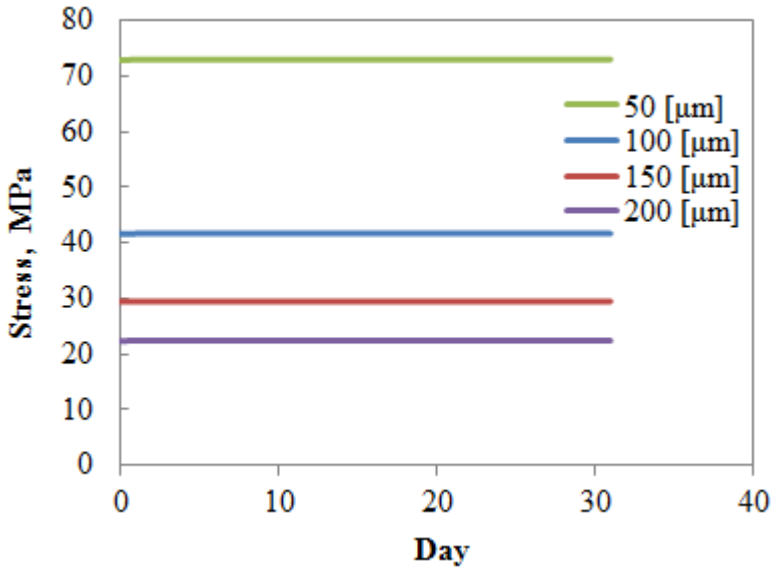

Fig. 12 (b)

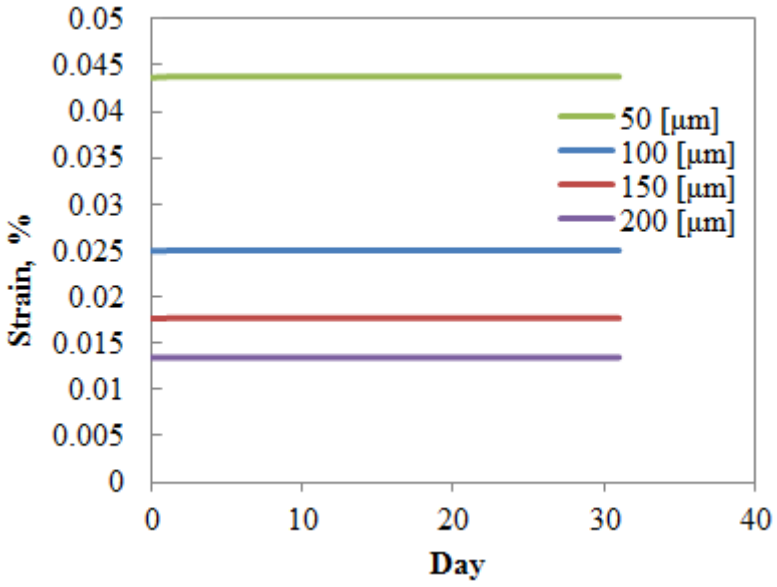

Fig. 13 (a)

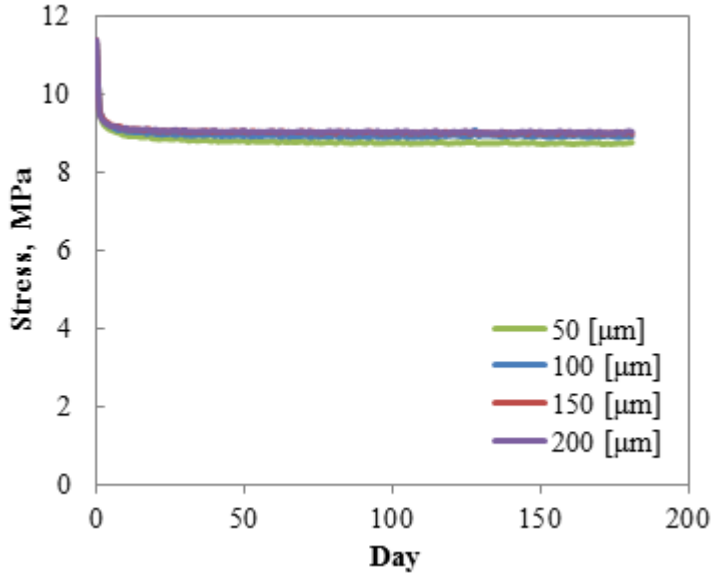

Fig. 13 (b)

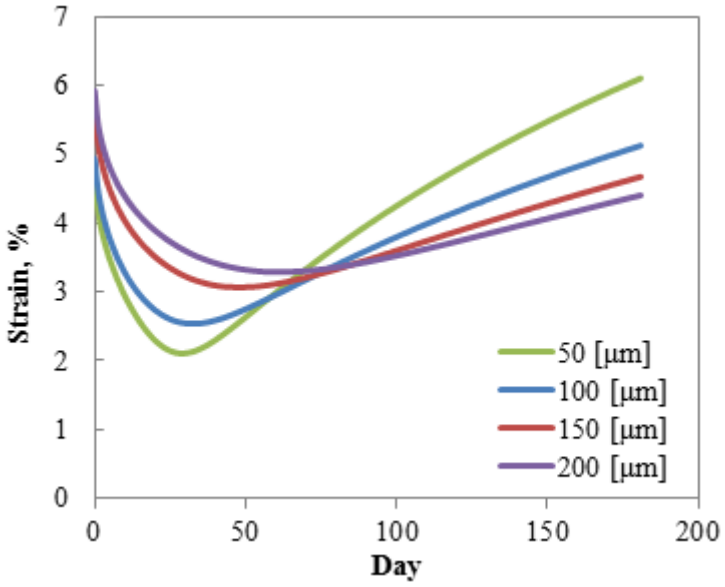

Table Legends

Table 1 Dimensions of materials of the FEM model.

Table 2 Changes in the thickness of silicon

Table 3 Relaxation modulus and relaxation time for CF.

Table 4 Temperature change during using conditions. (a)288K↔338K (b)278K↔318K (c)298K↔338K

Table 1

Model Dimensions	Si	CF	Lead-free solder	Tab line
Thickness, μm	200	25	25	200
Length, mm	152	152	152	152

Table 2

(a) Changes in the thickness of silicon				
Changes in parameters	Case name			
	Basic Model	Case 1	Case 2	Case 3
Thickness of silicon (μm)	200	150	100	50

Table 3

	G_i [Mpa]	t_i [s]
G_e	18.52	
G_1,t_1	76.04167226	1.67719E-17
G_2,t_2	66.64145084	1.93474E-16
G_3,t_3	70.32219498	2.23184E-15
G_4,t_4	73.7978527	2.57456E-14
G_5,t_5	79.62871406	2.96991E-13
G_6,t_6	88.64931451	3.42596E-12
G_7,t_7	105.5638331	3.95205E-11
G_8,t_8	136.2689132	4.55893E-10
G_9,t_9	190.1902796	5.259E-09
G_{10},t_{10}	273.2235596	6.06656E-08
G_{11},t_{11}	290.8875059	6.99814E-07
G_{12},t_{12}	130.6660281	8.07278E-06
G_{13},t_{13}	34.74453208	9.31243E-05
G_{14},t_{14}	8.230024055	0.001074244
G_{15},t_{15}	5.927283979	0.012392045

Table 4

Days (Hours)	Temperature (K)		
	298～338 K	288～338 K	278～318 K
0 (0)	298	288	278
0.041 (1)	338	338	318
0.5 (12)	338	338	318
0.541 (13)	298	288	278
1 (24)	298	288	278
1.041 (25)	338	338	318
1.5 (36)	338	338	318
1.541 (37)	298	288	278
2 (48)	298	288	278
2.041 (49)	338	338	318
2.5 (60)	338	338	318
2.541 (61)	298	288	278
3 (72)	298	288	278